

## **Predicting Snow-to-Liquid Ratio in the Mountains of the Western United States**

Peter G. Veals<sup>1</sup>, Michael Pletcher<sup>1</sup>, Andrew J. Schwartz<sup>2</sup>, Randy J. Chase<sup>4</sup>, Kirstin Harnos<sup>3</sup>,  
Jimmy Correia<sup>3</sup>, Michael E. Wessler<sup>5</sup>, and W. James Steenburgh<sup>1</sup>

<sup>1</sup>Department of Atmospheric Sciences, University of Utah, Salt Lake City, UT

<sup>2</sup>Central Sierra Snow Laboratory, University of California Berkeley, Soda Springs, CA

<sup>3</sup>NOAA/NWS/Weather Prediction Center, College Park, MD

<sup>4</sup>Cooperative Institute for Research in the Atmosphere, Colorado State University, Fort Collins,  
CO

<sup>5</sup>National Weather Service Western Region Headquarters, Salt Lake City, UT

Submitted to *Weather and Forecasting*

5 December 2024

Revised 6 April 2025

*Corresponding author address:* Peter G. Veals, Department of Atmospheric Sciences, University of Utah, 135 South 1460 East Room 819, Salt Lake City, UT, 84112. E-mail: peter.veals@utah.edu

1 **Abstract**

2 The snow-to-liquid-ratio (SLR) and its inverse, snow density, are crucial for forecasting  
3 snowfall in numerical weather prediction models and for estimating snow-water-equivalent (SWE)  
4 on the ground using remote sensing. SLR also varies widely in space and time, making it  
5 challenging to forecast accurately, particularly in the heterogenous terrain and climate of the  
6 mountains of the western United States. This study utilizes high quality, manually-collected  
7 measurements of new snowfall and new SWE from 14 mountainous sites across the region to build  
8 multiple linear regression (MLR) and random forest (RF) algorithms to predict SLR as a  
9 function of atmospheric variables.

10 When an MLR algorithm is trained on a simple combination of wind speed and temperature  
11 from either the ERA5 reanalysis, the GFS, or the HRRR, it predicts SLR with considerably more  
12 skill than existing SLR prediction methods. When a more extensive set of variables is considered,  
13 the skill improves further.

14 The variables used to achieve the most skillful prediction of SLR are temperature, wind  
15 speed, relative humidity, specific humidity, maximum solar altitude angle during the observing  
16 period, CAPE, and HRRR QPF. When an RF algorithm is trained using these variables, it can  
17 predict SLR with  $R^2=0.43$  and MAE=2.94. For the existing SLR prediction techniques currently  
18 used in operations,  $R^2$  ranges from 0.04 to 0.23 and MAE ranges from 4.01 to 9.45. Therefore  
19 the algorithms built in this paper can drastically improve SLR prediction over the mountains of  
20 the western US.

## 32 **1. Introduction**

33           Snowstorms in the western United States are essential for providing the water that sustains  
34 life, agriculture, industry, and hydropower in the region (Diffenbaugh et al. 2015; Li et al. 2017;  
35 Hagenstad et al. 2018). They can also pose a serious hazard to life, property, and commerce  
36 (Blattenberger and Fowles 1995; Spencer 2009; Black and Mote 2015; Seeherman and Liu 2015).  
37 Therefore, the accurate prediction and estimation of snowfall is essential, yet it remains difficult  
38 and error-prone.

39           Freshly-fallen snow is mostly air, with a snow-to-liquid ratio (SLR) ranging from 2:1 or  
40 lower to as high as 100:1 (e.g. Judson and Doesken 2000; Roebber et al. 2003). Consequently, for  
41 a given amount of liquid precipitation, the corresponding amount of snow can vary widely. This  
42 is a problem because contemporary snowfall prediction typically involves converting the liquid  
43 precipitation equivalent forecast that is directly predicted by numerical forecast systems (referred  
44 to as a quantitative precipitation forecast or QPF) to snow amount using an SLR (Alcott and  
45 Steenburgh 2000; Roebber et al. 2003; Byun et al. 2008; Pletcher et al. 2024). Conversely, for a  
46 given amount of snow, the corresponding amount of liquid can vary widely, posing a challenge  
47 for snow surveys and analyses that ingest the depth of new snowfall, yet seek to estimate the  
48 amount of liquid that has fallen (e.g., Raleigh and Small 2017). Therefore, the accurate prediction  
49 of SLR is essential to properly forecast snowfall and to measure snow-water-equivalent (SWE)  
50 from snow depth.

51           There are many factors that influence SLR. For example, the ice crystal habit can affect  
52 how densely crystals will pack together, increased riming of crystals removes some air space, high  
53 winds and the resulting ice crystal collisions can remove crystal branches causing tighter packing  
54 of crystals, natural compaction of snow under its own weight can densify it, and melting or rainfall  
55 can fill the spaces between crystals with water (Pomeroy and Brun 2001; Roebber et al. 2003;  
56 Baxter et al. 2005; Byun et al. 2008; Alcott and Steenburgh 2010; Steenburgh 2023). All of these  
57 processes are not explicitly or reliably accounted for in operational numerical forecast systems,  
58 motivating the need for other approaches to predict SLR.

59           Although SLR is known to vary, the simplest approach is to assume a fixed SLR. In the  
60 past, and even for convenience today, an SLR of 10:1 was/is sometimes assumed. The 10:1 rule  
61 was based on the findings of a single study conducted in eastern Canada that found a median SLR  
62 of 10 (Potter 1965; Roebber et al. 2003). However, not only is an SLR of 13 more appropriate for

63 most of the US (Baxter et al. 2005), using a fixed SLR can be problematic over regions like the  
64 western US where significant intra- and inter-storm SLR variability occurs (Judson and Doesken  
65 2000; Alcott and Steenburgh 2010; Pletcher et al. 2024).

66 To enable variable SLR prediction, the National Weather Service (NWS) National Blend  
67 of Models (NBM; Craven et al. 2020) uses four SLR methods referred to as 850–700-mb  
68 Thickness, Cobb, MaxTaloft, and Roebber in NWS training resources (Craven et al. 2020; The  
69 COMET Program 2023). The methods used and their weighting varies depending on the numerical  
70 modeling systems. The 850–700-mb Thickness method is used only for global ensembles and the  
71 data it requires would be subterranean at many western US sites, so it is not considered here. The  
72 Cobb method derives from Cobb and Waldstreicher (2005), although it has been revised several  
73 times. The Cobb method in NBM version 4.1 first identifies the maximum upward vertical  
74 velocity (UVV) contained in a cloudy layer, then calculates a weighting factor based on UVV and  
75 layer thickness, then applies a temperature-SLR relation to each model layer, and finally computes  
76 a weighted sum of the SLR from all model layers (The COMET program 2023). Most recently in  
77 NBM v4.2, a melting factor was added to adjust SLR based on the surface wet-bulb temperature  
78 and 1-h precipitation rate in marginal snow environments (Rudack et al. 2024).

79 The MaxTaloft SLR method is based on data from Alaska and uses a 5<sup>th</sup> degree polynomial  
80 to calculate SLR based on temperature:

$$\begin{aligned} \text{SLR}_{\text{MaxTaloft}} = & 0.0000045 * T_{\text{Max}}^5 + 0.0004432 * T_{\text{Max}}^4 + 0.0130903 * \\ & T_{\text{Max}}^3 + 0.0585968 * T_{\text{Max}}^2 - 1.8150809 * T_{\text{Max}} + 5.9805722, \end{aligned} \quad (1)$$

81 where  $T_{\text{Max}}$  is the maximum temperature (°C) between 610 m AGL and 400 hPa (The  
82 COMET Program 2023; Pletcher et al. 2024).

83 The Roebber method is derived from Roebber et al. (2003) who trained an artificial neural  
84 network using snowfall observations from NWS sounding sites and input variables that include  
85 monthly solar radiation, temperature and relative humidity at multiple levels, wind speed, and 6-h  
86 SWE. The training data consisted primarily of data from the eastern two-thirds of the US (the only  
87 western US sites were Great Falls, Lander, Salt Lake City, and Denver, all in in non-mountain  
88 areas of the western interior). The artificial neural network predicted SLR in three classes [heavy  
89 (1:1 < ratio < 9:1), average (9:1 ≤ ratio ≤ 15:1), and light (ratio > 15:1)], but was modified to  
90 produce a deterministic SLR for the NBM (The COMET Program 2023).

91 The Kuchera method, although not used in the NBM, is often used by forecasters and  
92 meteorological websites. As stated in Rosenow et al. (2023): “The so-called Kuchera method has  
93 become commonplace in operational meteorology, including the NWS, despite having not been  
94 formally published. This technique was created by performing a linear regression on snow depth  
95 and liquid equivalent observations using the maximum temperature in a column below 500  
96 hPa,  $T_{max}$ , as the sole predictor of SLR”. The Kuchera algorithm is defined as:

$$\text{SLR}_{\text{Kuchera}} = \begin{cases} 12 + 2 \times (271.16 - T_{max}), & T_{max} > 271.16 \\ 12 + (271.16 - T_{max}), & T_{max} \leq 271.16 \end{cases} \quad (2)$$

97  
98 Other SLR methods, based on a single air temperature variable, abound. Van Cleave (2013)  
99 relies on 700 hPa temperature, and a method recently implemented in the HRRR model (Benjamin  
100 et al. 2021) uses the temperature in the lowest model layer. Byun et al. (2008) use the 2 m  
101 temperature.

102 There are also a number of subregional SLR methods, such as that developed by Hoopes  
103 et al. (2023) for the mountain ranges of southern Arizona using gridded SLR analyses derived  
104 from Broxton et al. (2019). SLR in this case, however, is based on the 24-h change in the total  
105 depth of the snowpack divided by the 24-h change in snowpack SWE, which is a problematic due  
106 to compaction of the pre-existing snowpack.

107 These legacy SLR methods have not been carefully evaluated over the western US.  
108 However, Pletcher et al. (2024) compared the performance of the NBM SLR methods to a random  
109 forest algorithm trained on local data at one western US site: Alta Ski Area in the Wasatch Range  
110 of northern Utah. They found that the random-forest SLR algorithm produced substantially better  
111 SLR forecasts than the NBM methods, suggesting that an algorithm based on high quality regional  
112 observations might yield substantial forecast improvements for SLR over the western US.

113 One issue that affects nearly all of the SLR algorithms created to date is the paucity of  
114 high-quality snowfall and SWE (therefore SLR) observations from conventional meteorological  
115 networks like the NWS Cooperative Observer Program (COOP; Mehta 2023) and Automated  
116 Surface Observing Station (ASOS; NOAA 1998). Most of the datasets used to build these SLR  
117 algorithms use SWE from precipitation gauges, and when precipitation is falling as snow,

118 precipitation gauges suffer from a problem known as undercatch, whereby wind flowing up and  
119 over the gauge orifice prevents many hydrometeors from falling into the gauge (Rasmussen et al.  
120 2012). Undercatch is nonexistent during calm conditions, but grows with increasing wind speed.  
121 MacDonald and Pomeroy (2007) showed that for just an  $8 \text{ ms}^{-1}$  wind speed, an unshielded gauge  
122 will only capture  $\sim 30\%$  of the SWE that falls, and a gauge with an Alter shield will only capture  
123  $\sim 60\%$  of the SWE that falls. Thériault et al. (2012) suggest that undercatch is likely even greater  
124 than this, especially when the snowflakes have little riming. Compounding this issue, gauge SWE  
125 amounts from the National Weather Service Cooperative Summary of the Day (COOP) do not  
126 distinguish between SWE produced by snow or other precipitation types (e.g., ice pellets or liquid  
127 precipitation), adding additional uncertainty to snowfall measurements.

128 Another issue affecting legacy SLR algorithms is the fact that many of them were trained  
129 using observations mostly or completely from non-mountainous regions. Hydrometeor growth  
130 over mountainous regions is heavily influenced by the regions of ascent over the windward slopes  
131 of the terrain, with the majority of hydrometeor growth often happening  $< 2 \text{ km}$  above ground level  
132 (AGL) on these slopes. Storms in the interior ranges of the Western US also generally feature a  
133 temperature profile that decreases monotonically with height (e.g., Geerts et al. 2015; Aikins et al.  
134 2016; Friedrich et al. 2021). However, the dynamics of mountain waves, precipitation spillover,  
135 and flow blocking can often make for complex and difficult-to-predict accumulation patterns that  
136 can be far removed from the windward slopes (e.g., Neiman et al. 2002; Yuter et al. 2011; Geerts  
137 et al. 2015; Veals et al. 2020). Over flatter regions like the eastern half of the US, midlatitude  
138 cyclones generally produce the majority of cool-season precipitation. The hydrometeors in these  
139 cyclones can see much of their growth occur  $> 50 \text{ km}$  away from their eventual accumulation  
140 location, can be lofted along the way, and often originate  $7 \text{ km}$  or more AGL. They also often  
141 feature complex temperature profiles, with warm layers and inversions (e.g., Lackmann and  
142 Thompson 2019; Janiszski et al. 2024). Yet these are general differences, with a broad spectrum  
143 of atmospheric conditions possible for both flatland and mountain regions.

144 In this study, we develop algorithms to predict SLR over the western US using high-  
145 quality, manually measured snowfall and SWE observations from 14 geographically and  
146 climatologically diverse mountain observing sites. In Section 2, we describe the characteristics of  
147 these sites and observations, the techniques used to generate SLR algorithms, and the methods  
148 employed for verification. Section 3 then examines the fidelity of these algorithms, which exhibit

149 significant improvement relative to NBM SLR methods based on randomized testing, and  
150 examines the role of the atmospheric variables in predicting SLR. Section 4 summarizes the main  
151 conclusions, which illustrate the value of SLR algorithms based on high-quality regional data.

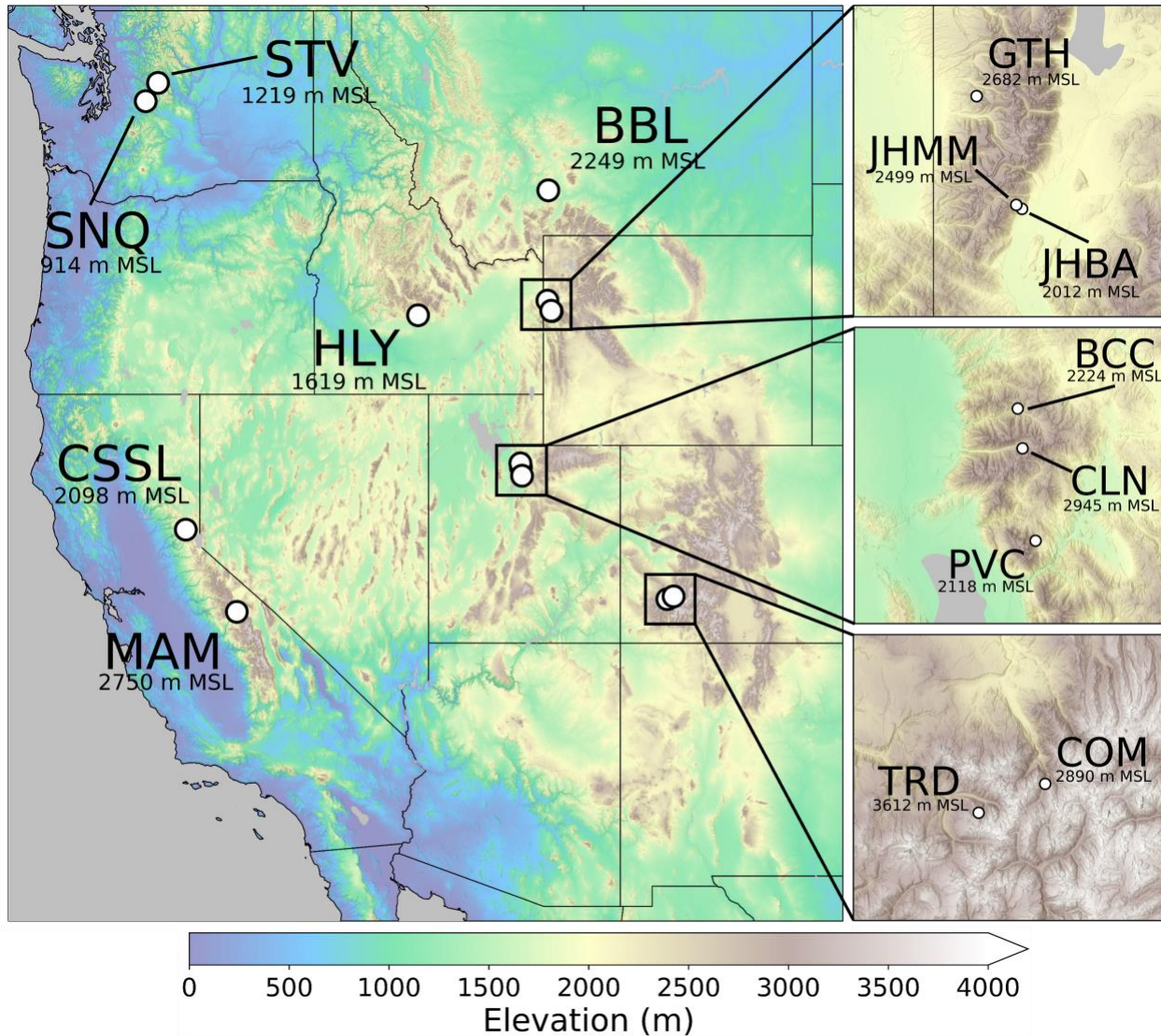
152

## 153 **2. Data and Methods**

### 154 *a. Snowfall Observations*

155 Data were obtained from 14 sites across the western US (Fig. 1, Table 1) where an observer  
156 takes manual observations of new snowfall and new SWE once or twice daily from a board that is  
157 wiped clean after each observation and placed atop the snowpack. SWE is based on a sample  
158 collected on the board by a coring tube and scale. This reduces errors due to undercatch, although  
159 high-wind situations can still create representativeness errors in some circumstances. Twelve of  
160 the observations come from snow-safety (i.e., avalanche mitigation) teams working for  
161 departments of transportation on avalanche-prone highways or at ski resorts where avalanche  
162 mitigation is frequently conducted. The remaining datasets are HLY, operated by an avalanche  
163 forecaster at the Sawtooth Avalanche Center, and CSSL, the Central Sierra Snow Laboratory  
164 ([cssl.berkeley.edu](http://cssl.berkeley.edu)). To mitigate the influence of rounding and measurement errors on SLR  
165 calculations, we only used observations from periods with snowfall  $> 5.08$  cm and SWE  $> 0.28$   
166 cm. These thresholds are consistent with prior studies (Judson and Doesken 2000; Roebber et al.  
167 2003; Alcott and Steenburgh 2010; Pletcher et al. 2024). We omitted observations (186 total) with  
168 SLR=10.0, as there were some cases in which the observer likely used 10.0 as a placeholder due  
169 to a missing depth or SWE observation. We tried omitting observations with SLR=20.0, as they  
170 appeared much more frequently than observations with SLR=19.0 or SLR=21.0, but omitting them  
171 did not significantly affect our results, so we chose to keep them. Careful investigation suggested  
172 that the increased frequency of SLR=20.0 reflects a tendency for observers, when measuring  
173 snowfall amounts  $\leq 4$  in (10.2 cm; the raw observations are taken in inches at most sites), to round  
174 the SWE amount to either 0.15 in (.38 cm) or 0.2 in (0.51 cm). Observations with  $SLR \leq 2$  and  
175  $SLR > 50$  were also omitted, as values in these ranges are more prone to rounding and/or  
176 measurement error.

177



178

179 Figure 1. Topography (m MSL following scale at bottom) of the Western US, with the locations of each of the  
 180 14 observing sites used in this study, and their elevations indicated.  
 181

Site	Data Available	Elevation (m)	Approx. Observation Frequency	<i>N</i> Observations
BBL	2018–2024	2249	24 h	177
BCC	2018–2024	2224	10 h and 14 h	234
CLN	2018–2024	2945	12 h	444
COM	2018–2024	2890	24 h	170
CSSL	2021–2024	2098	8 h and 16 h	170

GTH	2018–2020, 2022–2024	2682	24 h	155
HLY	2019–2024	1619	24 h	48
JHBA	2018–2024	2012	24 h	108
JHMM	2018–2024	2499	24 h	232
MAM	2018–2024	2750	6–18 or 24 h*	177
PVC	2018–2024	2118	11 h and 13 h	144
SNQ	2018–2024	914	24 h	271
STV	2020–2024	1219	24 h	176
TRD	2018–2024	3612	24 h	194

182 Table 1. For each of the 14 sites in this study, the name, period that data is available, elevation, approximate  
183 observation frequency, and number of observations used. \*MAM observations are most often ~24 h, but during  
184 intense storms, 2 observations per day are taken, with intervals ranging from ~6–18 h.  
185

186 The period of record varies widely among the sites, but we limit the data to the study period  
187 2 October 2018 – 30 April 2024 for all sites. The beginning date was selected because it marks the  
188 beginning of HRRR data availability beyond forecast hour 18, which is required for our analysis.  
189 Therefore, data for all sites comes from the full study period, except for CSSL, GTH, HLY, and  
190 STV, which had some missing seasons in the study period (Table 1). Within the study period, we  
191 only consider the heart of the cool season, which we define as the months of November–April.  
192 This leaves 2700 total observations that are used in this study.

193

#### 194 *b. Atmospheric Variables*

195 We build and evaluate one algorithm that uses atmospheric variables from the ERA5  
196 reanalysis (Hersbach et al. 2020), another algorithm that uses the High-Resolution Rapid Refresh  
197 model (HRRR; Benjamin et al. 2016), and another algorithm that uses the Global Forecast System  
198 model (NOAA EMC, 2024). The selection of atmospheric variables to consider in our algorithm  
199 was influenced by prior studies (e.g., Roebber et al. 2003; Alcott and Steenburgh 2010), the physics  
200 of ice crystal growth and metamorphism, and the available variables from the datasets used. These  
201 include:

- 202 (1) Temperature (T), specific humidity (Q), relative humidity (RH), and wind speed (SPD)  
203 linearly-interpolated from pressure coordinates to height AGL in increments of 400 m,  
204 spanning the surface to 4800 m AGL. The use of AGL coordinates makes the algorithm  
205 applicable at all elevations and grid points (pressure levels like 850 hPa are underground  
206 at many high elevation grid points, and 700 hPa may be near the surface at high elevations  
207 but 3 km above the flatlands and valleys). “T04” is used to denote T at 400 m AGL, “Q12”  
208 for Q at 1200 m AGL, “SPD24” for SPD at 2400 m AGL, and so on.
- 209 (2) Cloud-top temperature (CTT). The cloud top was defined as either (A) the location of the  
210 maximum RH lapse rate, or (B) the first location, moving upward from the 2<sup>nd</sup> pressure  
211 level above ground, where first RH drops below 80% for 2 consecutive levels.
- 212 (3) Solar altitude angle (Solar) during the observation period. We considered the mean and  
213 maximum, with the maximum having the strongest effect on SLR. Hereafter, we use the  
214 variable name “Solar” to denote the maximum solar altitude angle during the observing  
215 period.
- 216 (4) SWE amount – both the model-forecasted (hereafter QPF) and observed amounts.
- 217 (5) Temperature lapse rate – 1-2 km, 2-3 km, 3-4 km, 1-3 km, and 3-5 km AGL.
- 218 (6) Convective Available Potential Energy (CAPE) – as calculated and output by the  
219 modelling/reanalysis system

220 The process for attributing the atmospheric variable to the corresponding period of the SLR  
221 observation was as follows. To attribute the ERA5 reanalysis data to a 12-hour SLR observation,  
222 the mean of the ERA5 data within that 12-hour observation period is used. For a 24-hour  
223 observation, the mean of the ERA5 data within that 24-hour observation period is used, and so on  
224 for 8-hour observations, 16-hour observations, etc.

225 For the GFS and HRRR, which are forecasts, the process was slightly different. We began with  
226 the assumption that any forecast hour before Forecast Hour 10 (Fhr10) was of limited utility in a  
227 real-world setting, as it provides very little lead time for consumers of the forecast to make plans  
228 or decisions. We then tested two different time matching schemes:

- 229 (1) Only use data from the model initialization closest to the observation period, for which the  
230 observation period can fit entirely between Fhr10 and Fhr42.
- 231 (2) Assemble a timeseries of only Fhr12-Fhr24 from only 00Z and 12 model initializations,  
232 which creates one continuous timeline of atmospheric data.

233 Both method 1 and method 2 performed similarly for SLR prediction, so we opted for method 2  
234 because it was much easier to deal with for coding, data management, and understanding any issues  
235 when debugging was required. For all datasets, we experimented with the mean, maximum, and  
236 minimum value of the atmospheric variables during the observation period from the gridpoint  
237 nearest the observing site, and found the mean to be best for predicting SLR.

238

### 239 *c. SLR Algorithm*

240 We create four different SLR algorithm versions in this study, referred to as V1–V4. For  
241 V1 and V2, the atmospheric variables described above were fed into a multiple linear regression  
242 (MLR) calculator from the *scikit-learn* Python package (Pedregosa et al. 2011), along with the  
243 SLR observations from our 14 sites, to produce a predictive algorithm for SLR. For V3 and V4, a  
244 random forest (RF; Breiman 2001) regressor from *scikit-learn* is used instead to produce the  
245 predictive algorithm. To select the optimal hyperparameters for the RF, we began with the default  
246 values, including: 100 trees, no constraint on the maximum depth of the tree, a minimum of 2  
247 samples required to split a node, a minimum of 1 sample per node. We then experimented with a  
248 broad range of values for these hyperparameters, and none of the other values achieved a better  
249 predictive skill, so the default values are used in this study.

250 We chose the MLR technique because it is computationally inexpensive, easy to share, and  
251 easy to implement in any coding language. We chose the RF because, for input consisting of >6  
252 atmospheric variables, the resulting algorithm exhibits greater skill than the corresponding MLR  
253 algorithm in predicting SLR, can learn nonlinear relationships, and has been useful in other  
254 meteorological tasks (e.g., Pletcher et al. 2024; Chase et al. 2023 and references therein). We also  
255 experimented with other machine learning techniques, including Support Vector Regression  
256 (SVR; Vapnik 1995), and a type of neural network known as a Multilayer Perceptron (MLP;  
257 Gardner and Dorling 1998). We did not include the SVR in this work because it was an order of  
258 magnitude slower than the RF, making it unsuitable for forecasting applications, and we did not  
259 include the MLP because it was less skillful than the RF for our application.

260 All four algorithms (V1–V4) were built using a 60/40 train/test split, where 60% of the  
261 data (randomly selected) are used to train the algorithm, and the remaining 40% that have been  
262 withheld are used to test the performance of the algorithm. We evaluate the algorithm using the  
263 40% of observations that have been withheld for testing, and the evaluation is done 1000 times

264 (i.e. k-fold cross validation with  $k=1000$ ). This sampling procedure is done because the split into  
265 the 60/40 train/test observations is random, and the resulting algorithm and its performance can  
266 depend to some extent on which observations are dealt into testing or training. By doing 1000  
267 permutations of the train/test split process, we can account for this variability when evaluating  
268 algorithm performance. We consider the mean performance of the 1000 splits as a good estimate  
269 of model skill. Because observations from the same site that are adjacent to each other in time (for  
270 example the 00Z and 12Z observations from the same day) may occur under similar atmospheric  
271 conditions, it is possible that including an observation in the testing dataset and its temporally  
272 adjacent counterpart in the training dataset would artificially inflate the skill of the algorithm. We  
273 tried omitting any observations from testing that had a temporally adjacent counterpart in training,  
274 and it did not substantially affect our results, so we opt to permit temporally adjacent observations  
275 to keep a larger sample size.

276

#### 277 *d. NDFD data*

278 We obtained SLR forecasts from the NWS's National Digital Forecast Database (NDFD)  
279 for all cool seasons (November through April) in the entire period of record, which yielded the  
280 cool season from November 2020 through April 2024. The NDFD is a gridded dataset consisting  
281 of the forecasts sent out by each NWS forecast office. To compute SLR from the NDFD, we divide  
282 the forecast hour 6-12 snowfall by the forecast hour 6-12 SWE accumulation, and then make a  
283 continuous timeseries of SLR from these 6-12 hour forecasts. The data for each site come from  
284 the nearest NDFD gridpoint to the site.

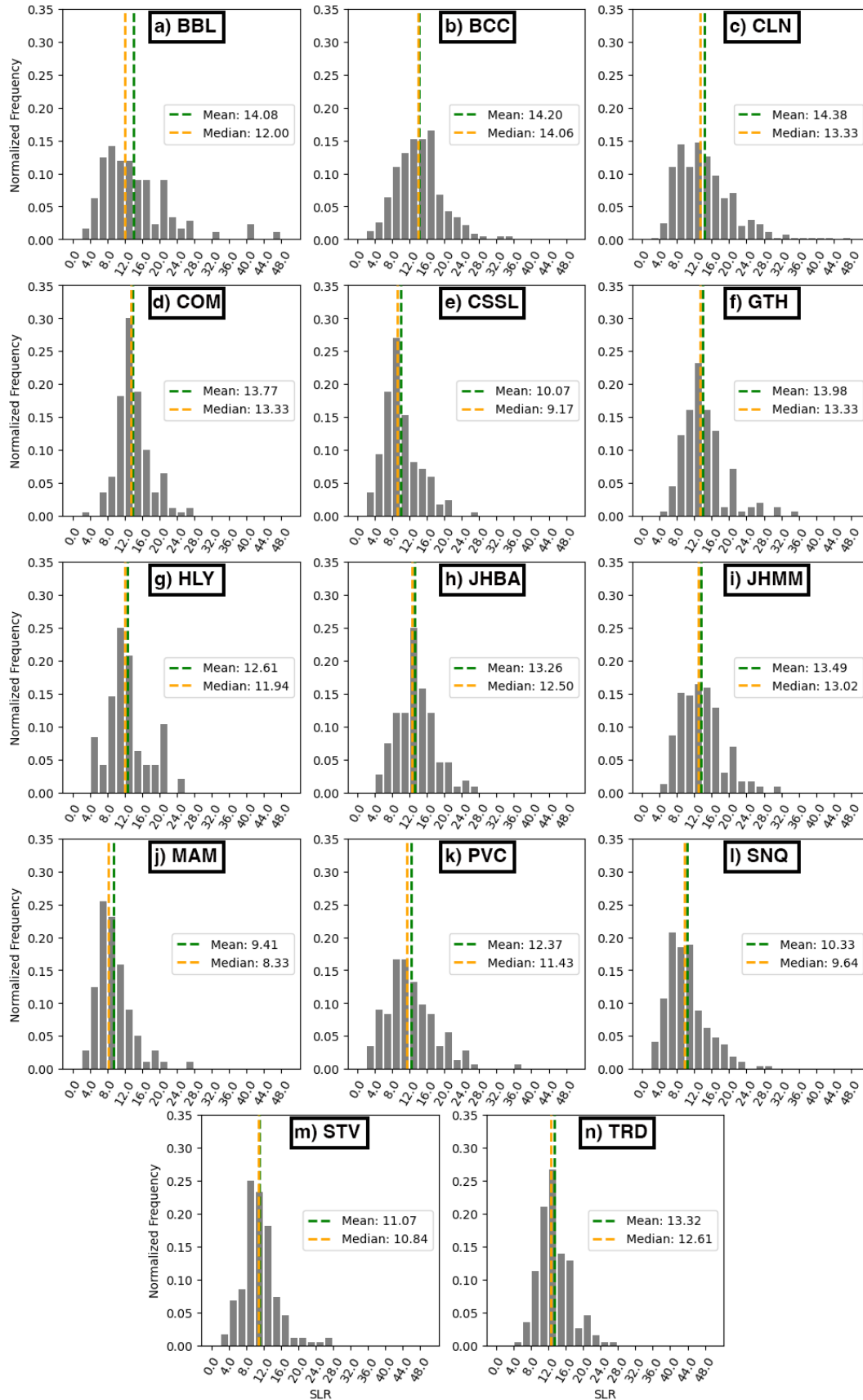
285

### 286 **3. Results**

#### 287 *a. Climatology of the 14 sites*

288 The distribution of SLR from each site over its period of record is shown in Fig. 2, with  
289 observations limited to those with snowfall  $> 5.08$  cm, SWE  $> 0.28$  cm, SLR  $> 2.0$ , SLR  $< 50$ , and  
290 SLR  $\neq 10.0$ . The sites in the Sierra Nevada and Cascade mountains (CSSL, MAM, SNQ, and  
291 STV), with their maritime snow climates (Trujillo and Molotch 2014), exhibit the lowest mean  
292 SLRs and narrowest SLR distributions (Fig. 2e,j,l,m). Although their SLR distributions are heavily  
293 skewed toward the lower values, they do still occasionally see events with SLR  $> 20$ . Farther inland,

294 COM and TRD have greater mean and median SLRs, and tails extending more to the right (Fig.  
295 2d,n). Moving farther north and/or farther inland to BBL, BCC, CLN, GTH, JHBA, JHMM, and  
296 PVC, where colder storms are more common, the distributions and tails move even farther to the  
297 right, with SLRs >20 being quite common (Fig 2 a,b,c,f,h,i,k). However, even at these cold  
298 continental locations, there are still a significant number of dense snow events with SLR <6,  
299 highlighting the broad variability from storm to storm at these locations. The effects of the  
300 interaction between synoptic climatology and terrain orientation can also be seen when comparing  
301 2 sites in the Wasatch Range of Utah (BCC and PVC). BCC is <26 km from PVC, and both sites  
302 are at nearly the same elevation, yet PVC has a much lower median and mean SLR than BCC and  
303 CLN. The primary difference is that PVC receives a much greater fraction of its cool season SWE  
304 from southwesterly flow events, which tend to be warmer and windier than other flow directions  
305 (Steenburgh 2023). The effects of elevation on snow climate are also apparent when comparing  
306 SNQ and STV, which are <45 km from one another, yet STV has significantly higher mean and  
307 median SLRs. STV is 300 m higher in elevation, which appears to have a strong impact on SLRs  
308 in the relatively warm maritime climate of the Cascades.

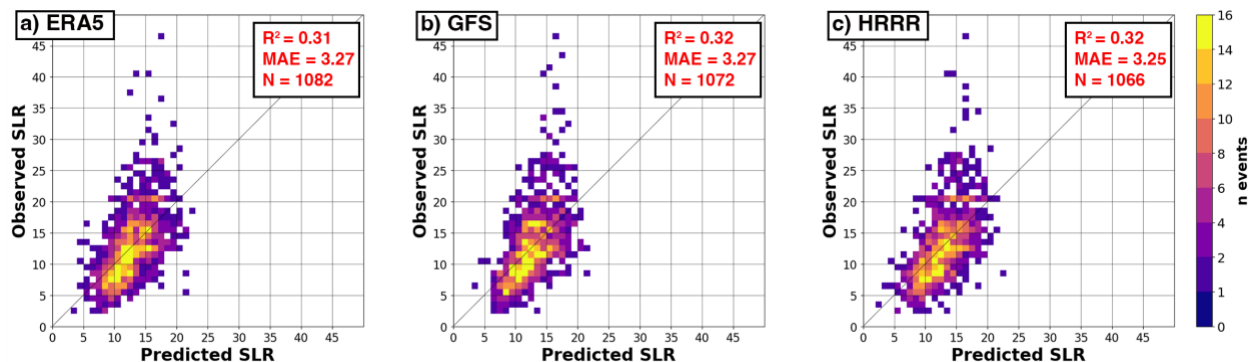


310 Figure 2. Distribution of observed SLR for the full period of record at each of the 14 sites used in this study.  
311 Note that at each site, observations with  $SLR=10.0$ ,  $SLR \leq 2.0$ ,  $SLR \geq 50$ ,  $SWE \leq 2.8$  mm, and snowfall  $\leq 50.8$   
312 mm have been removed.  
313

### 314 *b. V1 Algorithm*

315 We began by creating a simple version of the algorithm (V1) that yielded the best possible  
316 skill using only temperature and wind speed to train an MLR. It only requires 4 variables (T04,  
317 SPD04, T24, and SPD24), with the addition of extra levels yielding negligible additional skill. We  
318 evaluate skill using  $R^2$  and mean absolute error (MAE), with R being defined here as the Pearson  
319 correlation coefficient (Wilks 2019).

320 For our V1 algorithm, using data from ERA5, the mean  $R^2$  value for predicted SLR relative  
321 to observed SLR is 0.31, and the mean MAE value is 3.27, with the standard deviation ( $\sigma$ ) of the  
322 MAE at 0.07. Figure 3a shows a run of the algorithm that produced  $R^2$  and MAE values equal to  
323 the mean of the 1000 train/test iterations. The predicted SLR most closely matches observed SLR  
324 for low and moderate SLR values, but for events when observed SLR is  $>20$ , the spread increases  
325 (Fig. 3a).



326  
327 Figure 3. Observed SLR vs SLR predicted by the V1 algorithm, evaluated against the 40% of observations that  
328 are withheld from training to be used for testing, using (a) ERA5 reanalysis, (b) GFS, and (c) HRRR as the  
329 source of atmospheric input variables, shown here for one of the 1000 permutations for which  $R^2$  and MAE were  
330 equal to the mean  $R^2$  and mean MAE of the 1000 permutations.  
331

332 When the V1 algorithm is trained and tested the same way, but instead using GFS (Fig. 3b)  
333 and HRRR (Fig. 3c) data, the performance is nearly identical. The mean  $R^2$  and MAE using GFS  
334 data are 0.32 and 3.27, respectively. The mean  $R^2$  and MAE using HRRR data are 0.32 and 3.25,  
335 respectively. The similar performance between the ERA5, GFS, and HRRR suggests the  
336 differences in their depictions of temperature and wind speed values are not large enough to

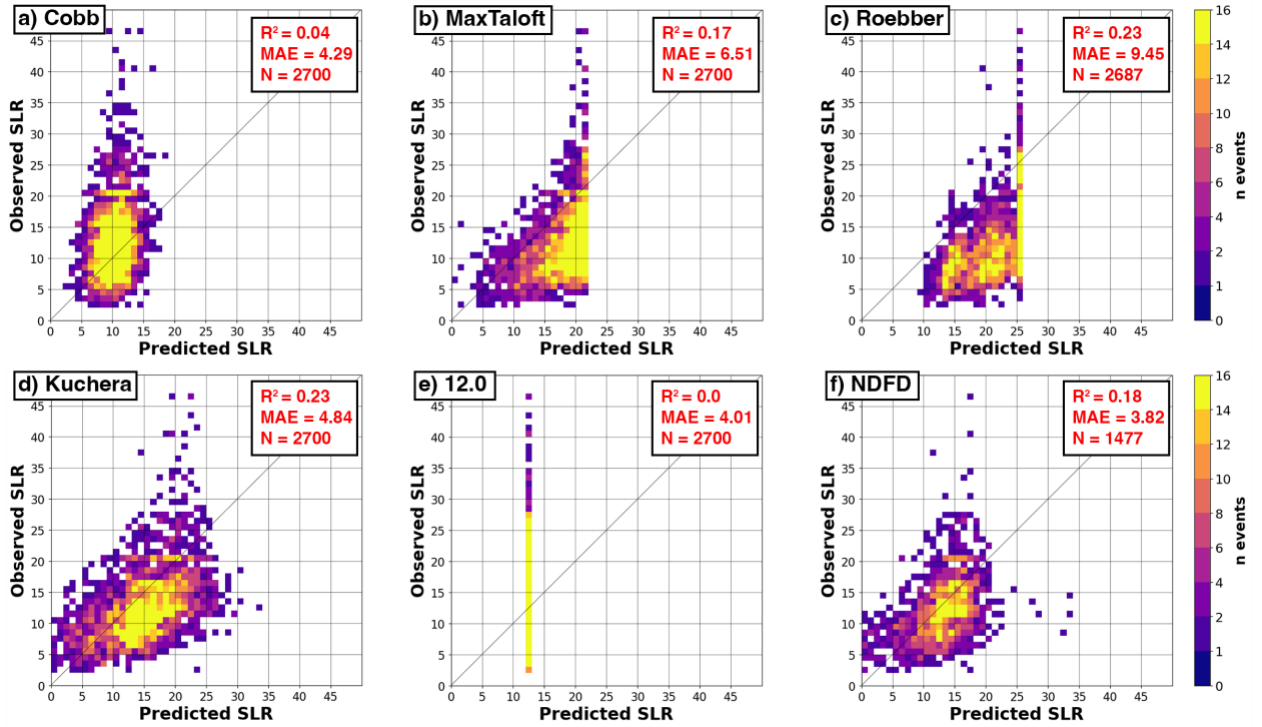
337 appreciably affect the skill of SLR prediction for the V1 algorithm.

338

339 *c. Legacy SLR methods*

340 We also computed SLR with 5 commonly used methods for comparison: (1) MaxTaloft,  
341 (2) Cobb, (3) Roebber, [all used operationally in NBM (Craven et al. 2020) v4.2], (4) the Kuchera  
342 method (described above), and (5) a fixed SLR. A sixth source of SLR, the forecast from the  
343 NDFD, is included, as it reflects the final SLR that goes out to users of NWS forecasts.

344 When the Cobb method is applied to the HRRR data for each of the cases in our 2018-2024  
345 study period, and compared to the high-quality manual observations from our dataset,  $R^2=0.04$  and  
346  $MAE=4.29$  (Fig. 4a). The SLR values predicted by Cobb are mainly clustered in the 5-15 range,  
347 with large prediction errors and very little correlation with reality. It is also biased a bit low,  
348 tending to underpredict SLR compared observed. Cobb's poor performance at these sites may be  
349 a result of the different distribution of vertical velocities, both in reality and in the HRRR, over  
350 complex terrain compared to flatter terrain. There may also be a different relationship between the  
351 location of hydrometeor growth and where the resulting hydrometeors reach the ground, over  
352 complex terrain compared to flatter terrain (see discussion of these difference near the end of  
353 Section 1). In other words, an algorithm that relies on vertical velocity locations and values  
354 observed over flat land may not perform well over complex terrain.



355  
356  
357  
358  
359

Figure 4. Observed SLR vs SLR from common sources of SLR prediction: (a) Cobb, (b) MaxTaloft, (c) Roebber, (d) Kuchera, (e) fixed 12.0 SLR, and (f) the NWS NDFD. No random test/training split needed for these datasets, so the total number of available observations are used.

360 When the MaxTaloft method is applied to the HRRR data for each of the cases in our 2018-  
361 2024 study period, and compared to the manual observations from our dataset, the  $R^2=0.17$  and  
362 MAE=6.51 (Fig 4b). MaxTaloft appears to greatly overpredict SLR (a high bias), with an even  
363 larger MAE than Cobb, and it rarely predicts SLR<10.0. The abrupt cutoff at ~22 reflects the  
364 boundary of MaxTaloft's polynomial formula.

365 When the Roebber method is applied to the HRRR data for each of the cases in our 2018-  
366 2024 study period, and compared to the manual observations from our dataset, the  $R^2=0.23$  and  
367 MAE=9.45 (Fig 4c). The predictions are biased quite high, with large prediction errors. The cluster  
368 of predictions at 25 reflects the fact that the NBM code caps the Roebber SLR prediction, with any  
369 prediction >25 set to 25.

370 When the Kuchera algorithm is applied to the HRRR data for each of the cases in our 2018-  
371 2024 study period, and compared to the observations from our dataset, the  $R^2=0.23$  and MAE=4.84  
372 (Fig 4d). The predicted SLR does exhibit some vague correlation with observed SLR, but the  
373 prediction errors are quite large and biased high.

374 Using a fixed SLR of 12.0 yields  $R^2=0.0$  and  $MAE=4.01$  (Fig. 4e). We experimented with  
375 fixed SLR values from 10.0 to 13.0, in increments of 0.1, and 12.0 yielded the best performance  
376 in our dataset. This differs of course from the 10.0 that is commonly used for a fixed SLR, likely  
377 due to the fact that many of the sites in our dataset have mean and median SLRs around 12, 13, or  
378 even 14 (Fig 2).

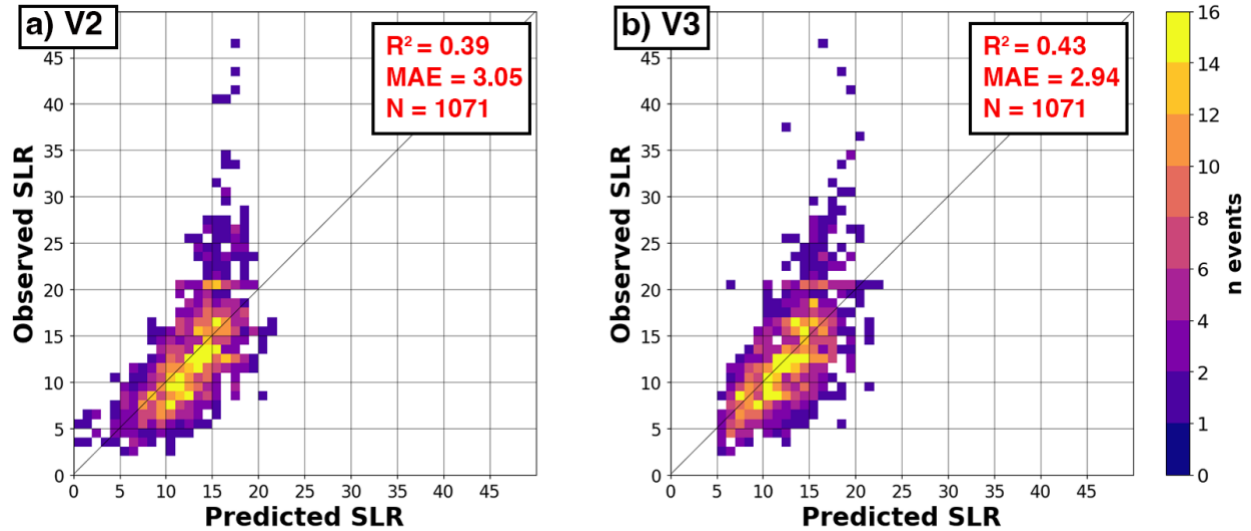
379 The final SLR that we evaluate is the forecast SLR from the NDFD. When compared to  
380 our observations, the  $R^2=0.18$  and  $MAE=3.82$  (Fig 6f). This is the lowest MAE and best  
381 performance of the 6 legacy SLR techniques. The NDFD is a gridded aggregate of the forecasts  
382 issued by each NWS office, so the methods used to produce the final SLR values varies with time  
383 and by office, but the NDFD SLR outperforms all of the NBM SLR techniques. It does not,  
384 however, outperform the V1 algorithm.

385

#### 386 *d. V2 and V3 Algorithms*

387 To build the V2 algorithm, we began with the variables described in Section 2b and used  
388 recursive elimination, stepwise screening regression, and lasso regression (Wilks 2019) to identify  
389 the optimal set of input variables from the HRRR, selecting for the lowest MAE and highest  $R^2$   
390 value relative to observed SLR. The combination of variables that added skill to the algorithm  
391 includes: T04, SPD04, SPD24, RH04, RH24, Q04, Q24, model QPF, CAPE, and Solar. When  
392 these variables are input into an MLR, the performance of the V2 algorithm improves relative to  
393 V1, with  $R^2=0.39$  and  $MAE=3.05$  (Fig. 5a). This includes some improvement in predicting SLRs  
394  $>20$ , although these events remain a challenge. In practical terms, the algorithm does not have the  
395 ability to discriminate between the conditions associated with an observed SLR of 15 and those  
396 associated with an SLR of 25.

397



398

399 Figure 5. Observed SLR vs SLR predicted by (a) the V2 and (b) V3 algorithms, evaluated against the 40% of  
 400 observations that are withheld from training to be used for testing, shown here for one of the 1000 permutations  
 401 for which  $R^2$  and MAE were equal to the mean  $R^2$  and mean MAE of the 1000 permutations.  
 402

403

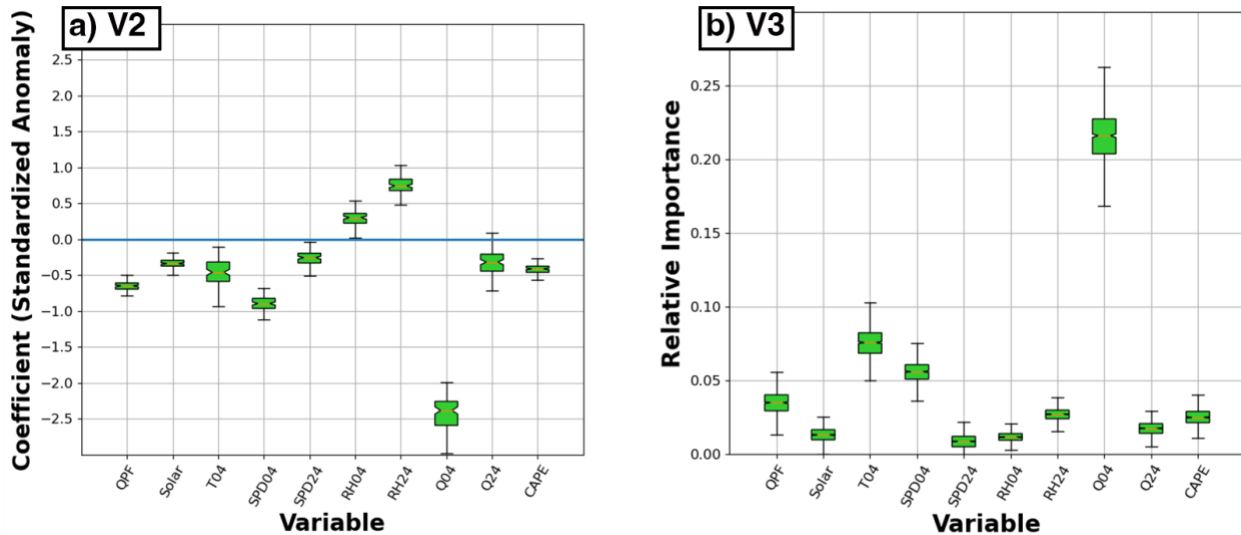
404 The V3 algorithm uses a RF regressor instead of MLR to increase skill. This V3 of the  
 405 algorithm, when compared to observed SLR, yields  $R^2=0.43$  and  $MAE=2.94$  (Fig 5b). The  
 406 increased skill of V3 relative to V2, given the same set of input variables, is a result of the RF's  
 407 ability to detect and replicate nonlinear relationships between the input variables and SLR. The  
 408 relationships predicted by the MLR are, by definition, linear. Even though V3 is more skillful than  
 409 V2 on the whole, there is little or no improvement in anticipating the high SLR events (Fig 5b).

410

411 *e. Importance of each variable*

412 The logical next step in this study is to explore the importance of each variable to the fit of  
 413 the algorithm. For V2, which is an MLR, the algorithm must be re-run using the standardized  
 414 anomaly of each variable, rather than its actual value. This does not change the fit or skill of the  
 415 algorithm; it simply makes the coefficient of each term in the regression equation represent the  
 416 relative contribution of its corresponding variable to the fit of the equation. The train/test split and  
 417 the MLR fit are performed 1000 times and the coefficients recorded for each of these 1000  
 418 permutations. This process determines that Q04 (400 m AGL specific humidity) to have the  
 419 greatest contribution to the MLR equation with a median coefficient of -2.3 (Fig 6a). A negative

420 coefficient indicates SLR decreases with increasing Q04. The next most important variable is 400  
 421 m AGL wind speed (SPD04), with a median coefficient of -0.8, followed by RH24 with a median  
 422 coefficient of 0.7, and HRRR QPF with a median coefficient of 0.65 (Fig 6a).  
 423



424  
 425 Figure 6. (a) For the V2 algorithm, with all atmospheric input variables from the HRRR converted to  
 426 standardized anomalies, the coefficients for each term in the MLR equation. The magnitude of a coefficient is  
 427 proportional to its importance in predicting SLR in the equation. The box-and-whisker plots represent the 1000  
 428 different values of the coefficient for the 1000 permutations. (b) For the V3 algorithm, the importance of each  
 429 variable in the Random Forest regression. The box-and-whisker plots represent the different values of the  
 430 coefficient for the 1000 permutations. The differences between boxes are statistically significant at the 95%  
 431 confidence interval if the notches area around the medians do not overlap.  
 432

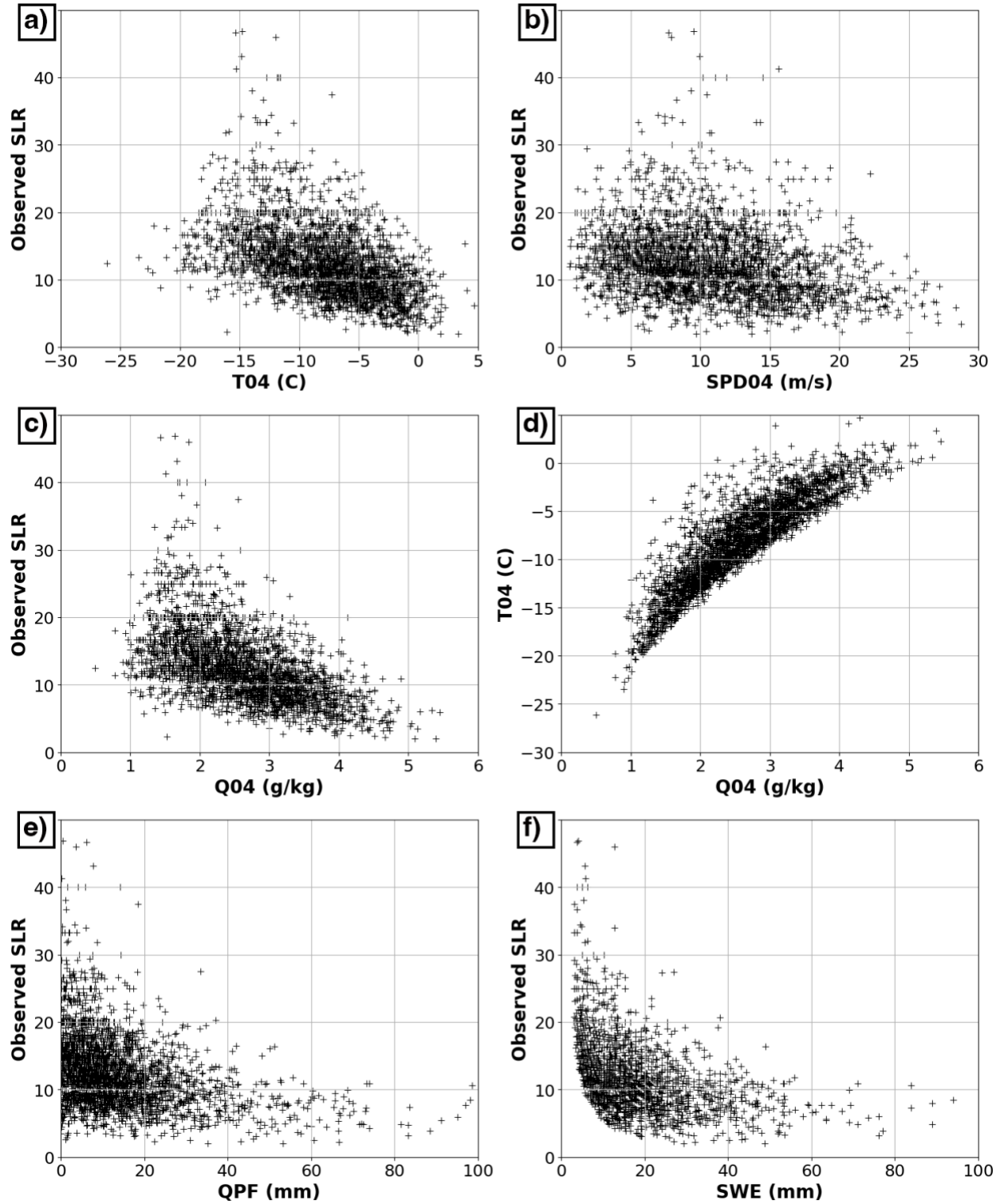
433 The importance of each variable in the RF version of algorithm V3, as again determined  
 434 by 1000 permutations, looks somewhat different than for the MLR. The scoring of relative  
 435 importance is also determined differently for the RF, with the nonlinear fits for each variable  
 436 making it impractical to assign a single sign to the contribution of the variable. So feature  
 437 importance for the RF is determined by the contribution to model fit when the values in a column  
 438 are randomly reshuffled (Breiman 2001). As in the MLR algorithm, Q04 is again the greatest  
 439 contributor to the fit by a wide margin, with a median relative importance of 0.24 (Fig 6b). Then  
 440 in a distant 2<sup>nd</sup>, 3<sup>rd</sup>, and 4<sup>th</sup> place are T04, SPD04, and HRRR QPF, respectively. The main contrast  
 441 with the MLR relative importances is that T04 has a much more prominent role (2<sup>nd</sup> most important  
 442 variable) in the RF than it does in the MLR. This suggests that when temperature is permitted to  
 443 have a nonlinear fit, it more accurately predicts SLR.

444

445 *f. Relationships amongst variables*

446 For the most important atmospheric variables identified in the previous section, the key  
447 relationships amongst them and with observed SLR are explored next. The observed SLR exhibits  
448 an increasing trend with decreasing T04 up until values of around -15 C, when the relationship  
449 changes sign and colder values actually tend to yield increasing SLR (Fig 7a). Something  
450 resembling this can be seen in a number of prior studies (Byun et al. 2008; Alcott and Steenburgh  
451 2010). It suggests that when T04 is colder than about -15 C, the temperature in the zone where  
452 most crystals are growing (likely at or above the 400 m AGL level where T04 is defined) is cold  
453 enough that dendritic crystals are no longer favored, and crystal habits that pack more densely,  
454 like plates and columns, are beginning to be favored. See Nakaya (1954) and Bailey and Hallett  
455 (2009) for more information on favored crystal habit as a function of temperature.

456



457

458 Figure 7. For all observations, (a) observed SLR vs T04, (b) observed SLR vs SPD04, (c) observed SLR vs Q04,  
 459 (d) T04 vs Q04, (e) observed SLR vs QPF, and (f) observed SLR vs observed SWE.

460

461  
462  
463  
464  
465  
466  
467  
468  
469  
470  
471  
472  
473  
474  
475  
476  
477  
478  
479  
480  
481  
482  
483  
484  
485  
486  
487  
488  
489  
490  
491

The relationship between SPD04 and observed SLR is weaker, with a decreasing SLR trend with increasing SPD04 (Fig. 7a). This is due to the tendency for increasing wind speeds to fracture ice crystals, with the resulting fragments likely packing more densely than intact crystals (e.g., Steenburgh 2023). The relationship appears most useful for forecasting when values of SPD04 are  $\geq 20 \text{ ms}^{-1}$ . Under these conditions, only one instance of SLR  $> 20$  occurs in our dataset.

The relationship between Q04 and observed SLR is stronger than that of T04 and observed SLR (Fig. 7c). This is a bit surprising, as T04 and Q04 are very closely related (Fig 7d), with the Clausius-Clapeyron equation governing their relationship when the air is at saturation (Wallace and Hobbs 2006). The relationship between Q04 and observed SLR is also roughly the same shape (though the opposite sign) as that of T04 and observed SLR, with a trend reversal around  $Q04 \cong 1.5 \text{ g kg}^{-1}$ , below which observed SLR decreases. Yet an important factor appears to be that the trend reversal is not nearly as pronounced for Q04 as it is for T04. For moderate and high values of Q04, there is also much less variability in SLR for a given value of Q04 than there is for a moderate or high value of T04 (cf. 7a, 7c).

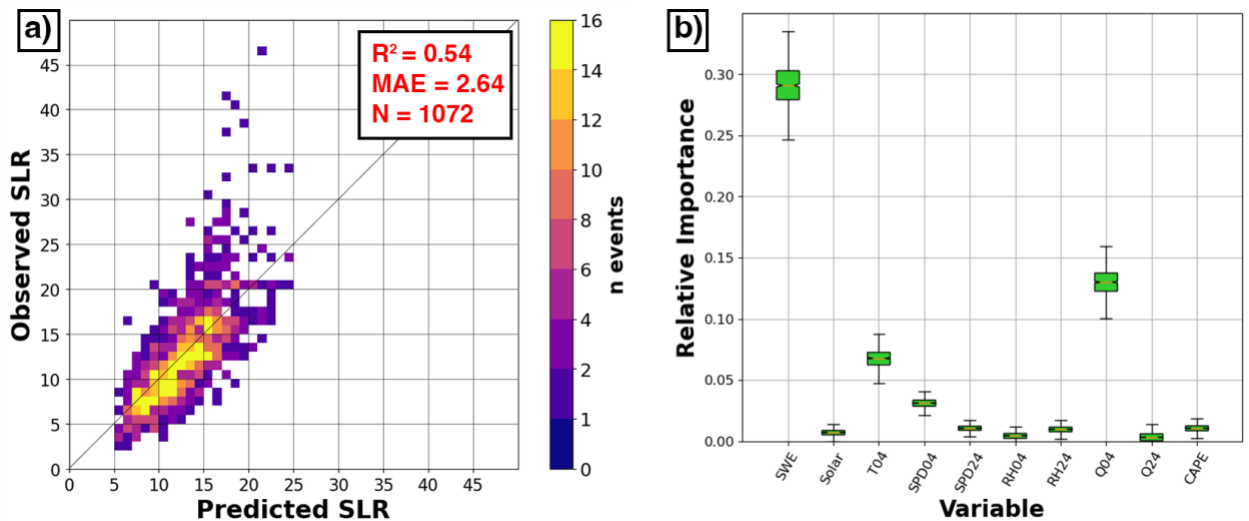
As for potential physical explanations of the Q04-SLR relationship, it is well established that at saturation in subfreezing clouds, increasing temperature (and therefore specific humidity) generally leads to increasing supercooled liquid water content (SLWC; e.g., Gultepe and Isaac 1997). Increasing SLWC, in turn, leads to increased riming (Waitz et al. 2022). Yet this would suggest temperature is just as important, at least near saturation, as specific humidity. This result is also at odds with previous studies, which conclude that temperature is more important. Therefore future work is needed to examine these physical processes, in particular the differences in snow growth over lowland regions compared to mountain regions.

HRRR QPF is negatively correlated with observed SLR (Fig 7e). This is likely due to the fact that an increasing amount of SWE on the interval board leads to increasing compaction of the entire column under its own weight. Supporting this assertion, the relationship between observed SWE and observed SLR is much stronger (Fig 7f). This means that for modelling systems with QPF forecasts that tend to be closer to reality, more skillful SLR prediction is possible. It also means that for non-forecasting applications, where observed SWE is available as a variable for SLR prediction, even greater forecasting skill than that of the V3 algorithm is possible.

492 *g. V4 Algorithm*

493 The V4 algorithm is identical to the V3 algorithm, except that it uses observed SWE instead  
 494 of HRRR QPF. As mentioned above, this is only useful for applications that are run after a snowfall  
 495 event is over, like snowfall analyses, in which observed SWE for the event is available.

496 The V4 algorithm, when compared to observed SLR, predicts SLR with  $R^2=0.54$  and  
 497 MAE=2.64. (Fig 8a). When the feature importance is calculated for the algorithm, using 1000  
 498 permutations, observed SWE is the greatest contributor to the fit by a wide margin, with a median  
 499 relative importance of 0.28 (Fig 8b). Q04 is relegated to a distant 2<sup>nd</sup> place with a median  
 500 importance of 0.13, followed by T04 in 3<sup>rd</sup> place at 0.07. The most dramatic illustration of V4's  
 501 increased skill is how well it handles high SLR (>20) events (Fig 8a). It is clear that a major factor  
 502 contributing to the difficulty of V1–V3 in forecasting high SLR events is that QPF forecasts have  
 503 large errors. If SWE could be forecasted perfectly, high SLR events would not be nearly as  
 504 challenging to predict. SWE amount is the single most important variable in predicting SLR  
 505 accurately.



506

507 Figure 8. (a) Observed SLR vs SLR predicted by the V4 algorithm, evaluated against the 40% of observations  
 508 that are withheld from training to be used for testing, using HRRR as the source of atmospheric input variables,  
 509 shown here for one of the 1000 permutations for which  $R^2$  and MAE were equal to the mean  $R^2$  and mean MAE  
 510 of the 1000 permutations. (b) For the V4 algorithm, the importance of each variable in the Random Forest  
 511 regression. The box-and-whisker plots represent the different values of the coefficient for the 1000 permutations.  
 512 The differences between boxes are statistically significant at the 95% confidence interval if the notches area  
 513 around the medians do not overlap.

514

515 Because the V4 algorithm is trained with observed SWE, it is only skillful when it is

516 applied to observed SWE. If it is applied to model QPF, it performs poorly (not shown). This is  
517 because model QPF often deviates substantially from, and is biased compared to, observed SWE.  
518 For model QPF to add skill, the algorithm must be trained on model QPF (this is what V2 and V3  
519 are).

520

#### 521 **4. Summary and Conclusions**

522 This study utilizes a novel dataset of manually-collected snowfall and SWE measurements  
523 taken every ~24-h or less from an interval board placed atop the snowpack by snow safety workers  
524 and scientists at 14 sites across the western US. We then use these observations and atmospheric  
525 variables from either the ERA5, the GFS, or the HRRR to train a MLR or RF algorithm to predict  
526 SLR. A simple model utilizing only temperature and wind speed at 2 levels as the predictive  
527 variables (known as V1) performs well when compared to observed SLR events that were withheld  
528 from training the algorithm, with  $R^2=0.32$  and MAE=3.27 when using the GFS forecasts. When  
529 the training source was instead ERA5 reanalysis or HRRR forecasts, the  $R^2$  and MAE values were  
530 within 1% of the above values.

531 These  $R^2$  and MAE values from the simple V1 algorithm substantially outperform the 3  
532 SLR algorithms (Cobb, MaxTaloft, and Roebber) that are used operationally in the NBM version  
533 4.2. The respective  $R^2$  values for those algorithms, when compared to observed SLR values, are  
534 0.04, 0.17, and 0.23, with respective MAE values of 4.29, 6.51, and 9.45. The V1 algorithm also  
535 substantially outperforms a commonly used but unpublished algorithm known as the Kuchera  
536 method. When SLR predicted by Kuchera is compared to observed SLR,  $R^2=0.23$  and MAE=4.84.

537 There are several potential explanations for the poor performance of the 4 legacy SLR  
538 algorithms relative to observations. The first is that these 4 algorithms were trained partly or  
539 entirely on SLR observations for which the liquid equivalent came from a precipitation gauge, and  
540 precipitation gauges, even with an Alter shield, can undercatch falling snow by 40% or more  
541 (MacDonald and Pomeroy 2007; Thériault et al. 2012). Such undercatch would strongly affect the  
542 resulting SLR values. The observations used in our dataset are not immune to the effects of high  
543 winds, but using a weighed core from an interval board is substantially less error-prone than a  
544 precipitation gauge. Another issue is that algorithms like Cobb and MaxTaloft are mostly trained  
545 with variables from NWP over relatively flat terrain. In the complex terrain of the western US,  
546 steep slopes can dramatically increase or decrease vertical velocity, for example. Complex terrain

547 may also cause most crystal growth and riming to happen at different heights above ground level  
548 than they do over flat terrain. Furthermore, the synoptic climatology of the sites used in this study  
549 may differ from that of the cyclone-dominated central and eastern US.

550         The V1 algorithm also substantially outperforms two other sources of SLR forecasts. If a  
551 fixed 12.0 SLR is used (12.0 yielded the best performance for our dataset) and compared to  
552 observed SLR,  $R^2=0.0$  and  $MAE=4.01$ . The SLR forecasts from the NDFD are obtained for the 4  
553 cool seasons that they are available from the archive (2020–2024) and compared to observed SLR.  
554  $R^2=0.18$  and  $MAE=3.82$ . The NDFD is a gridded aggregate of the forecasts issued by each NWS  
555 office.

556         We trained the V2 and V3 algorithms on the optimal combination of atmospheric variables  
557 from the HRRR to achieve the maximum possible skill, as defined by  $R^2$  and MAE. The optimal  
558 combination of variables was T04, SPD04, SPD24, RH04, RH24, Q04, Q24, model QPF, CAPE,  
559 and Solar. The V2 algorithm is a MLR trained with these variables, and when its forecasted SLR  
560 is compared to observed SLR from a set of data points withheld for testing, the resulting  $R^2$  and  
561 MAE are 0.39 and 3.05, respectively. The V3 algorithm is a RF model trained with the same  
562 variables. When V3 algorithm, which contains complex nonlinear relationships to predictive  
563 variables, is used to build an algorithm, the resulting  $R^2$  and MAE are 0.43 and 2.94, respectively.  
564 For both the V2 and V3 versions of our algorithm, the most important variable is Q04 by a wide  
565 margin. In a distant 2<sup>nd</sup>, 3<sup>rd</sup>, and 4<sup>th</sup> place for importance in the V2 algorithm are SPD04, RH24,  
566 and model QPF, respectively. In a distant 2<sup>nd</sup>, 3<sup>rd</sup>, and 4<sup>th</sup> place for importance in the V3 algorithm  
567 are T04, SPD04, and model QPF, respectively. High SLR (>20) events are the most challenging  
568 for the algorithms, though these events account for 7% of the cases in the dataset.

569         The V4 algorithm is identical to V3, except that it uses observed SWE instead of HRRR  
570 QPF. This means it is only useful for applications that are run after a snowfall event is over, like  
571 snowfall analyses, in which observed SWE for the event is available. When forecasted SLR from  
572 V4 is compared to observed SLR from a set of data points withheld for testing, the resulting  
573  $R^2=0.54$  and  $MAE=2.64$ . The use of observed SWE as a predictor, instead of QPF, is responsible  
574 for the dramatic improvement in algorithm performance. The high SLR (>20) events do not pose  
575 nearly the forecasting challenge that they do for the V1, V2, and V3 algorithms. SWE becomes  
576 the most important variable by a wide margin, followed by Q04, T04, and SPD04 in a distant 2<sup>nd</sup>,  
577 3<sup>rd</sup>, and 4<sup>th</sup> place, respectively. This shows that much of the difficulty in forecasting high SLR

578 events is due to the uncertainty in QPF amounts. If QPF were a perfect forecast of SWE, high SLR  
579 events would not be nearly as difficult to predict.

580 In summary, the V1, V2, and V3 algorithms represent a large increase in skill for SLR  
581 prediction compared to the current algorithms and techniques used by forecasters, and the V4  
582 algorithm is quite skillful for non-forecasting applications. But these algorithms were only trained  
583 to mountain sites with colder temperatures, located closer to cloud base, and different synoptic and  
584 mesoscale weather conditions than much of the lowlands and flatlands of the US. Therefore, future  
585 work will include developing an algorithm trained on high-quality manual snowfall observations  
586 from the entire US. A final important caveat is that because most of the legacy SLR algorithms are  
587 trained using precipitation gauge observations that often suffer from undercatch, these algorithms  
588 may verify more favorably when evaluated with such gauge observations. Conversely, the  
589 algorithms we've developed may not perform as well when these gauge observations are treated  
590 as the "truth".

591

592

593 *Acknowledgements:* This research was supported by NOAA grants NA19OAR4590137,  
594 NA22OAR4590531, and NA23OAR4310278. Any opinions, findings, and conclusions or  
595 recommendations expressed in this paper are those of the authors and do not necessarily reflect  
596 the views of the funding organization. Analyses were performed using Python software packages.  
597 We thank MesoWest, NOAA, NCAR, Unidata, and the University of Utah Center for High  
598 Performance Computing for the provision of datasets, software, and computing resources. We also  
599 thank Ned Bair, Aaron Barnett, Frank Carus, Steven Clark, Mike Cooperstein, Ella Darham,  
600 Daniel Nagy, Carol Peck, Jon Preuss, Mike Rheam, Dave Richards, Harlan Sheppard, John  
601 Stimberis, Jon Tukman, and Alan Willard for all their hard work gathering and sharing data. Jesse  
602 Meng was a huge help in getting the NBM algorithms coded up.

603

604 *Data availability:* The HRRR data were obtained from Amazon Web Services  
605 (<https://registry.opendata.aws/noaa-hrrr-pds/>). GFS data were obtained from the National Center  
606 for Atmospheric Research's Research Data Archive (<https://rda.ucar.edu/datasets/d084001/>). The  
607 ERA5 data were obtained from the Copernicus Climate Change Service  
608 (<https://cds.climate.copernicus.eu/datasets/reanalysis-era5-pressure-levels?tab=overview>). The

609 NDFD data were obtained from Amazon Web Services (<https://noaa-ndfd->  
610 [pds.s3.amazonaws.com/index.html](https://noaa-ndfd-pds.s3.amazonaws.com/index.html)). The V1–V4 SLR algorithms are available on GitHub  
611 ([https://github.com/pveals/Veals\\_etal\\_2025](https://github.com/pveals/Veals_etal_2025)). The snowfall and SWE observations from CLN are  
612 available online from the University of Utah Research Data Repository  
613 (<https://hive.utah.edu/concern/datasets/0r967383v>). The CSSL and HLY observations are  
614 available on the GitHub ([https://github.com/pveals/Veals\\_etal\\_2025](https://github.com/pveals/Veals_etal_2025)), but due to their proprietary  
615 nature, the remainder of the snowfall and SWE observations are limited to access by verified  
616 researchers, and are available through the corresponding author.

617

618

619

620

621

## References

622

623 Aikins, J., K. Friedrich, B. Geerts, and B. Pokharel, 2016: Role of a Cross-Barrier Jet and  
624 Turbulence on Winter Orographic Snowfall. *Mon. Wea. Rev.*, **144**, 3277–3300.

625 Alcott, T. I., and W. J. Steenburgh, 2010: Snow-to-liquid ratio variability and prediction at a high-  
626 elevation site in Utah’s Wasatch Mountains. *Weather and Forecasting*, **25**, 323–337.  
627 <https://doi.org/10.1175/2009waf2222311.1>.

628 Bailey, M.P, and J. Hallett, 2009: A Comprehensive Habit Diagram for Atmospheric Ice Crystals:  
629 Confirmation from the Laboratory, AIRS II, and other Field Studies. *J. Atmos. Sci.*, **66**,  
630 2888–2899.

631 Baxter, M. A., C. E. Graves, and J. T. Moore, 2005: A Climatology of Snow-to-Liquid Ratio for  
632 the Contiguous United States. *Wea. Forecasting*, **20**, 729–744,  
633 <https://doi.org/10.1175/WAF856.1>.

634

635 Benjamin, S. G., and Coauthors, 2016: A North American hourly assimilation and model forecast  
636 cycle: The Rapid Refresh. *Mon. Wea. Rev.*, **144**, 1669–1694, doi:10.1175/MWR-D-15-

637 0242.1.  
638  
639 \_\_\_\_, and coauthors, 2021: Diagnostic fields developed for hourly updated NOAA weather models.  
640 NOAA technical memo OAR GSL-66, 54pp, [https://rapidrefresh.noaa.gov/Diag-vars-](https://rapidrefresh.noaa.gov/Diag-vars-NOAA-TechMemo.pdf)  
641 [NOAA-TechMemo.pdf](https://rapidrefresh.noaa.gov/Diag-vars-NOAA-TechMemo.pdf)  
642  
643 Black, A.W., and T.L. Mote, 2015: Characteristics of Winter-Precipitation-Related Transportation  
644 Fatalities in the United States. *Wea. Clim. Society*, **7**, 133-145.

645 Blattenberger, G., and R. Fowles, 1995: Road closure to mitigate avalanche danger: a case study  
646 for Little Cottonwood Canyon. *Int. J. Forecast.*, **11**, 159–174.

647 Breiman, L., 2001: Random Forests. *Machine Learning*, **45**, 5–32,  
648 <https://doi.org/10.1023/A:1010933404324>.

649 Broxton, P., X. Zeng, and N. Dawson, 2019: Daily 4 km gridded SWE and snow depth from  
650 assimilated in-situ and modeled data over the conterminous US, version 1. NASA  
651 National Snow and Ice Data Center Distributed Active Archive  
652 Center. <https://doi.org/10.5067/0GGPB220EX6A>

653 Byun, K., J. Yang, and T. Lee, 2008: A Snow-Ratio Equation and Its Application to Numerical  
654 Snowfall Prediction. *Wea. Forecasting*, **23**, 644–658,  
655 <https://doi.org/10.1175/2007WAF2006080.1>.  
656

657 Chase, R.J., D.R. Harrison, A. Burke, G.M. Lackmann, and A. McGovern, 2023: A Machine  
658 Learning Tutorial for Operational Meteorology. Part I: Traditional Machine Learning.  
659 *Wea. Forecasting*, **37**, 1509–1529.  
660

661 Cobb, D. K., and J. S. Waldstreicher, 2005: A simple physically based snowfall algorithm. *21st*  
662 *Conf. on Weather Analysis and Forecasting/17th Conf. on Numerical Weather Prediction*,  
663 Washington, DC, Amer. Meteor. Soc., 2A.2.  
664 <http://ams.confex.com/ams/pdfpapers/94815.pdf>.

665  
666 Craven, J. P., Rudack, D. E., and Shafer, P. E., 2020: National blend of models: A statistically post-  
667 processed multi-model ensemble. *J. Operational Meteor.*, **8**, 1–14,  
668 <https://doi.org/10.15191/nwajom.2020.0801>.

669 Diffenbaugh, N.S, D.A. Swain, and D. Touma, 2015: Anthropogenic warming has increased  
670 drought risk in California. *Proc. Nat. Acad. Sci*, **112**, 3931–3936.

671 Friedrich, K., and coauthors, 2021: Microphysical Characteristics and Evolution of Seeded  
672 Orographic Clouds. *J. Appl. Meteorol. Climatol.*, **60**, 909–934.

673 Gardner, M.W., and S.R. Dorling, 1998: Artificial neural networks (the multilayer perceptron) –  
674 a review of applications in the atmospheric sciences. *Atmos. Environment*, **32**, 14–15.

675 Geerts, B., Y. Yang, R. Rasmussen, S. Haimov, and B. Pokharel, 2015: Snow Growth and  
676 Transport Patterns in Orographic Storms as Estimated from Airborne Vertical-Plane  
677 Dual-Doppler Radar Data. *Mon. Wea. Rev.*, **143**, 644–665.

678 Gultepe, I., and G.A. Isaac, 1997: Liquid Water Content and Temperature Relationship from  
679 Aircraft Observations and Its Applicability to GCMs. *J. Climate.*, **10**, 446–452.

680 Hagenstad, M., E. Burakowski, and R. Hill, 2018: The economic contributions of winter sports  
681 in a changing climate. Report published by Protect our Winters.  
682 [https://protectourwinters.org/wp-content/uploads/2019/12/POW\\_EconReport\\_v22.pdf](https://protectourwinters.org/wp-content/uploads/2019/12/POW_EconReport_v22.pdf)

683 Hersbach, H., and coauthors, 2020: The ERA5 global reanalysis. *Q. J. Roy. Meteor. Soc.*, **146**,  
684 1999–2049.

685 Hoopes, C. A., C. L. Castro, A. Behrangi, M. R. Ehsani, P. Broxton, 2023: Improving prediction  
686 of mountain snowfall in the southwestern United States using machine learning methods.  
687 *Meteor. Appl.*, **30**, e2153, <https://doi.org/10.1002/met.2153>.

688  
689 Janiszkeski, A., R.M. Rauber, B.F. Jewett, and T. J. Zaremba, 2024: Reorganization of Snowfall

690 Beneath Cloud-top within the Comma Head Region of Two Extreme US East Coast Winter  
691 Cyclones. *Wea. Forecasting*, **39**, 1181–1202.

692 Judson, A., and N. Doesken, 2000: Density of freshly fallen snow in the central Rocky  
693 Mountains. *Bull. Amer. Meteor. Soc.*, **81**, 1577–1587.

694 Li, D., M.L. Wrzesien, M. Durand, J. Adam, and D. Lettenmaier, 2017: How much runoff  
695 originates as snow in the western United States, and how will that change in the future?  
696 *Geophys. Res. Lett.*, **44**, 6163–6172.

697 MacDonald JP, JW Pomeroy, 2007: Gauge Undercatch of Two Common Snowfall Gauges in a  
698 Prairie Environment. In *Proceedings of the 64th Eastern Snow Conference*, St. John's,  
699 Newfoundland, Canada: 119–126.

700 Mehta, A., 2023: Requirement and Standards for NWS Climate Observations.  
701 [https://www.weather.gov/media/directives/010\\_pdfs/pd01013002curr.pdf](https://www.weather.gov/media/directives/010_pdfs/pd01013002curr.pdf)

702 Nakaya, U., 1954: *Snow Crystals: Natural and Artificial*. Harvard University Press, 510 pp.

703 Neiman, P. J., F. M. Ralph, A. B. White, D. E. Kingsmill, and P. O. G. Persson, 2002: The  
704 Statistical Relationship between Upslope Flow and Rainfall in California's Coastal  
705 Mountains: Observations during CALJET. *Mon. Weather Rev.*, **130**, 1468–1492.

706 NOAA, 1998: Automated Surface Observing System (ASOS) User's Guide.  
707 <https://www.weather.gov/media/asos/aum-toc.pdf>.

708 NOAA EMC, 2024: The Global Forecast System. Accessed 31 January 2024,  
709 [https://www.emc.ncep.noaa.gov/emc/pages/numerical\\_forecast\\_systems/gfs/documentati](https://www.emc.ncep.noaa.gov/emc/pages/numerical_forecast_systems/gfs/documentati)  
710 [on.php](https://www.emc.ncep.noaa.gov/emc/pages/numerical_forecast_systems/gfs/documentati)

711

712 Pedregosa, F., and Coauthors, 2011: Scikit-Learn: Machine Learning in Python. *J. Mach. Learn.*  
713 *Res.*, **12**, 2825-2830. <https://doi.org/10.48550/arXiv.1201.0490>.

714  
715 Pletcher, M.D, and coauthors, 2024: Validation of cool-season snowfall forecasts at a high-  
716 elevation site in Utah’s Little Cottonwood Canyon. Early Online Release, *Wea and Forec.*  
717  
718 Pomeroy, J. W., and Brun, E., 2001: Physical properties of snow. *Snow Ecology*, H. G. Jones,  
719 Pomeroy, J. W., Walker, D. A., Hoham, R. W., Eds., Cambridge University Press, 45–126.  
720  
721 Potter, J. G., 1965: Water content of freshly fallen snow. Meteorology Branch, Dept. of Transport,  
722 CIR-4232, TEC-569, Toronto, ON, Canada, 12 pp. [Available from National Snow and Ice  
723 Data Center User Services, University of Colorado, Campus Box 449, Boulder, CO 80309-  
724 0449.]  
725  
726 Raleigh, M.S., and E.E. Small, 2017: Snowpack density modeling is the primary source of  
727 uncertainty when mapping basin-wide SWE with lidar. *Geophys. Res. Lett.*, **44**, 3700–  
728 3709.  
729  
730 Rasmussen, R., and Coauthors, 2012: How well are we measuring snow: The NOAA/FAA/NCAR  
731 Winter Precipitation Test Bed. *Bull. Amer. Meteor. Soc.*, **93**, 811–  
732 829, <https://doi.org/10.1175/BAMS-D-11-00052.1>.  
733  
734 Roebber, P.J., S. L. Bruening, D. M. Schultz, and J. V. Cortinas, 2003: Improving Snowfall  
735 Forecasting by Diagnosing Snow Density. *Wea. Forecasting*, **18**, 264–287,  
736 [https://doi.org/10.1175/1520-0434\(2003\)018<0264:ISFBDS>2.0.CO;2](https://doi.org/10.1175/1520-0434(2003)018<0264:ISFBDS>2.0.CO;2).  
  
737 Rosenow, A.A., H.D. Reeves, and D. Tripp, 2023: Evaluation of Ensemble Snowfall Forecasts  
738 Using Operationally Used Snow-to-Liquid Ratios in Five Winter Storms. *Wea. and*  
739 *Forec.*, **38**, 2135–2147.  
  
740 Rudack, D., R. James, S. Perfater, G. Manikin, and A. Just, 2024: National Blend of Models  
741 (NBM) v4.2 Upgrades and Improvements, 40 pp.  
742 [https://vlab.noaa.gov/documents/6609493/6665561/NBM\\_v4.2\\_Eval\\_SlideDeck.pdf](https://vlab.noaa.gov/documents/6609493/6665561/NBM_v4.2_Eval_SlideDeck.pdf)

743 Seeherman, J., and Liu, Y., 2015: Effects of extraordinary snowfall on traffic safety. *Accid.*  
744 *Anal. Prev.*, **81**, 194-203, <https://doi.org/10.1016/j.aap.2015.04.029>.

745 Spencer, J.M., 2009: Winter Weather Related Fatalities in the Conterminous United States: An  
746 Analysis of Three Winter Fatality Databases, M.S. Thesis, Dept of Geography, Northern  
747 Illinois University, 91 pp. [https://www.proquest.com/openview/4dfd6aff74007b6808](https://www.proquest.com/openview/4dfd6aff74007b68087582a4ffd811ea/1?pq-origsite=gscholar&cbl=18750)  
748 [7582a4ffd811ea/1?pq-origsite=gscholar&cbl=18750](https://www.proquest.com/openview/4dfd6aff74007b68087582a4ffd811ea/1?pq-origsite=gscholar&cbl=18750)

749

750 Steenburgh, W.J., 2023: *Secrets of the Greatest Snow on Earth*. 2<sup>nd</sup> Ed. Utah State University  
751 Press, 215 pp.

752

753 The COMET Program, 2023: Understanding NBM v4.0 snowfall products. The University  
754 Corporation for Atmospheric Research, 22 May 2024,  
755 [https://www.meted.ucar.edu/education\\_training/lesson/10166](https://www.meted.ucar.edu/education_training/lesson/10166).

756

757 Thériault, J., R. Rasmussen, K. Ikeda, and S. Landolt, 2012: Dependence of snow gauge  
758 collection efficiency on snowflake characteristics. *J. Appl. Meteor. Climatol.*, **51**, 745–  
759 762, <https://doi.org/10.1175/JAMC-D-11-0116.1>.

760

761 Thompson, G., and G.M. Lackmann, 2019: Hydrometeor Lofting and Mesoscale Snowbands.  
762 *Mon. Wea. Rev.*, **147**, 3879–3899.

763

764 Trujillo, E., and N.P. Molotch, 2014: Snowpack regimes of the Western United States. *Water*  
765 *Resour. Res.*, **50**, 5611–5623.

766

767 Vapnik, V., 1995: *The Nature of Statistical Learning*. Springer, 314pp.

768

769 Veals, P.G., W.J. Steenburgh, S. Nakai, and S. Yamaguchi, 2020: Intrastorm Variability of the  
770 Inland and Orographic Enhancement of a Sea-Effect Snowstorm in the Hokuriku Region  
771 of Japan. *Mon. Wea. Rev.*, **148**, 2527–2548.

772

773 Waitz, F., M. Schnaiter, T. Leisner, and E. Järvinen, 2022: In situ observations of riming in mixed-  
774 phase clouds using the PHIPS probe. *Atmos. Chem. Phys.*, **22**, 2087–7103.  
775

776 Wilks, D.S., 2019: *Statistical Methods in the Atmospheric Sciences*. Fourth Edition. Elsevier, 840  
777 pp.  
778

779 Yuter, S. E., D. A. Stark, J. A. Crouch, M. J. Payne, and B. A. Colle, 2011: The impact of  
780 varying environmental conditions on the spatial and temporal patterns of orographic  
781 precipitation over the Pacific Northwest near Portland, Oregon. *J.*  
782 *Hydrometeor.*, **12**, 329–351.  
783  
784